Tropical Journal of Pharmaceutical Research October 2026; 25 (10): 1333-1343
ISSN: 1596-5996 (print); 1596-9827 (electronic)

Available online at http://www.tjpr.org
https://dx.doi.org/10.4314/tjpr.v25i10.1

Original Research Article

Multi-objective optimization for quality control in 3D-printed pharmaceuticals: ensuring precision in drug layering

Muqdad Alhijjaj[1,2]*, Ahmed AA Alsaad[1] and Mustafa Sabah Taha[3]
[1]Department of Pharmaceutics, College of Pharmacy, University of Basrah, 61004 Basrah, [2]Department of Pharmaceutics, College of Pharmacy, Al-Kunooze University, 61026 Basrah, [3]Missan Oil Training Institute, Ministry of Oil, 61026 Missan, Iraq

For correspondence:* ***Email:* *muqdad.mousa@uobasrah.edu.iq*

Sent for review: 13 July 2026 *Revised accepted: 21 October 2026*

Abstract

Purpose: *To develop an optimized framework for quality control of 3D printing in pharmaceutical processes.*
Methods: *The framework integrated five key quality parameters: active pharmaceutical ingredient (API) content accuracy, uniformity, mechanical strength, production time, and dissolution profile.*
Results: *The proposed framework identified Pareto-optimal solutions where no objective can be improved without degrading at least one other. Solution 1 showed better content accuracy and uniformity, and superior mechanical properties at all infill densities, with about 15 % higher mechanical properties compared to solutions 2 and 3. Solution 1 had longer build times, especially at small layer heights, compared to solution 3. Solution 1 also showed good content uniformity but had significantly lower dissolution-profile accuracy and longer production time. Furthermore, none of these solutions has a dissolution profile that is very close to the target.*
Conclusions: *Evaluation of the proposed framework highlighted efficient identification of diverse parameter combinations that simultaneously satisfy multiple quality requirements; hence, the framework may inform manufacturing decisions based on specific priorities and regulatory constraints.*

Keywords: *Content uniformity, Drug layering precision, Multi-objective optimization, Pareto optimization, Pharmaceutical 3D printing*

This is an Open Access article that uses a funding model which does not charge readers or their institutions for access and distributed under the terms of the Creative Commons Attribution License (http://creativecommons.org/licenses/by/4.0) and the Budapest Open Access Initiative (http://www.budapestopenaccessinitiative.org/read), which permit unrestricted use, distribution, and reproduction in any medium, provided the original work is properly credited.

Tropical Journal of Pharmaceutical Research is indexed by Scopus, Chemical Abstracts, Embase, Index Copernicus, EBSCO, African Index Medicus, JournalSeek, Directory of Open Access Journals (DOAJ), African Journal Online, Bioline International, Open-J-Gate and Pharmacy Abstracts

INTRODUCTION

Three-dimensional (3D) printing has transformed pharmaceutical manufacturing by enabling rapid, on-demand production of personalized medicines with precise control over drug dose, release profiles, and incorporation of multiple active pharmaceutical ingredients (APIs). This flexibility is particularly valuable for pediatric and geriatric patients, whose therapeutic requirements vary considerably [1]. However, quality control (QC) remains a major barrier to the wider regulatory

© 2026 The authors. This work is licensed under the Creative Commons Attribution 4.0 International License

and scientific acceptance of 3D-printed pharmaceuticals. Conventional QC approaches designed for large-scale production and destructive end-product testing are poorly suited to low-volume and unit-dose manufacturing. The layer-by-layer (LBL) process can introduce variations in drug release, mechanical strength, layer thickness, geometry, and API distribution, all of which may affect therapeutic efficacy and patient safety [2,3].

Pharmaceutical production uses several 3D-printing technologies, including fused deposition modeling (FDM), stereolithography (SLA), selective laser sintering (SLS), inkjet printing, and semi-solid extrusion (SSE) [3], each with specific QC challenges. FDM can produce oral solid dosage forms but may experience inter-batch variation due to differences in filament diameter and extrusion temperature. The 3D objects produced by SLA and Digital Light (DL) printing often result in objects with high resolution; however, they encounter mechanical problems and drug uniformity issues. In addition, the energy of the laser and the scanning speed of SLA 3D printing have an impact on the release profile of the drug and the porosity of the resulting pharmaceutical product. On the other hand, inkjet printing is capable of producing structures with good drug uniformity, while SSE has the advantage of printing at room temperature and enables in-line drug content quantification [1,3].

Several non-destructive characterization tools have shown an important role in the analysis of pharmaceutical 3D-printed preparations. Raman and near-infrared (NIR) spectroscopy can detect the drug loading percentages without affecting the structure of the formulation. Equipment such as terahertz pulsed imaging (TPI) and micro-computed tomography (μ-CT) can evaluate the internal microstructure of the 3D objects. Scanning electron microscopy (SEM) can visualize the outer surface and the precision of the threads deposited during the build-up process. These tools provide in-line precision evaluation despite the limitations of their integration during the manufacturing process [4]. In pharmaceutical 3D printing, quality control is a complex interplay between advanced printing methods, critical quality parameters, and intelligent optimization frameworks (Figure 1).

This study examined the most important technologies (FDM, SLA, SLS, inkjet, and SSE) and evaluated some of the most important quality control parameters (mass and dose uniformity, layer thickness consistency, drug distribution fidelity, mechanical strength, and real-time process monitoring parameters; Figure 2). Each of these technologies has its own benefits and drawbacks, but there is one common challenge: scalable and adaptive QC strategies for achieving layer-level accuracy in a variety of production environments [5]. To address this challenge, integrative frameworks (such as multi-objective optimization approaches, which are less frequently used for pharmaceutical manufacturing research) are needed.

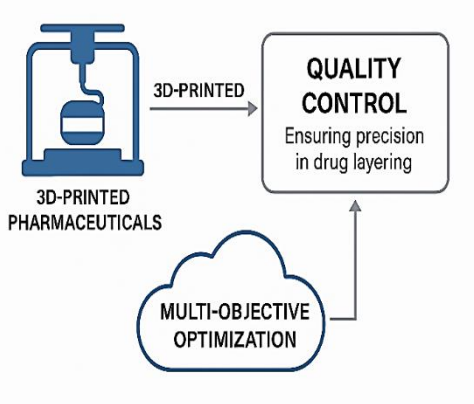


Figure 1: An illustration of the challenges facing QC for pharmaceutical dosage form development, correlating the technologies used in pharmaceutical 3D printing and the required critical attributes with multi-objective optimization (MOO)

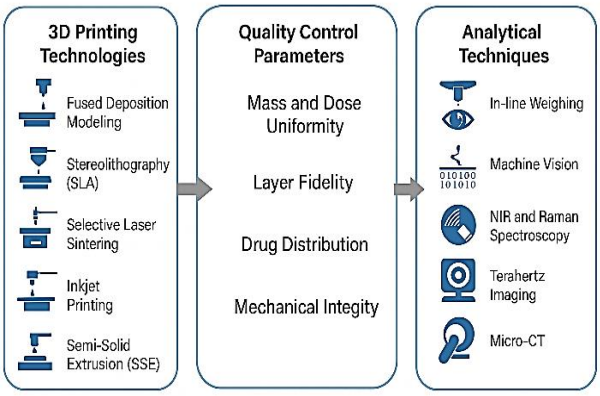


Figure 2: An overview of the quality control procedures, 3D-printing processing techniques and characterization equipment

There are several conflicting targets in 3D printing of pharmaceutical dosage forms. These include the accuracy of drug content, precision of printing, unnecessary waste of materials, optimal mechanical properties and compliance with the regulations. These interacted parameters can be solved potentially using multi-objective optimization. Algorithms such as the Non-dominated Sorting Genetic Algorithm II (NSGA-II) [6] and Multi-Objective Evolutionary Algorithm based on Decomposition (MOEA/D) [7] have

demonstrated effectiveness in other manufacturing fields. However, systematic application to pharmaceutical 3D printing remains largely unexplored. A previous study identified 6 gaps in integrating MOO algorithms with real-time QC tools to provide adaptive control of drug deposition and layer formation [8]. The need for a mathematically structured and adaptive QC framework capable of managing variability across 3D-printing processes while simultaneously optimizing multiple CQAs has also been suggested [9]. The aim of this study is to provide an optimization solution based on NSGA II that integrates the different competing parameters such as mechanical strength, drug content accuracy, manufacturing efficiency and regulatory compliance.

EXPERIMENTAL

Framework

This section presents the MOO framework for efficient QC in pharmaceutical 3D printing. It outlines the mathematical formulation of the problem and the development of a model that captures the critical relationships between process parameters and product quality. Furthermore, it describes the implementation of the NSGA-II followed by evaluation metrics for assessing the performance of the proposed MOO framework.

Problem formulation

It is assumed that $\Omega \subset \mathbb{R}^n$ represents a feasible parameter space for pharmaceutical 3D printing, wherein each point $\boldsymbol{x} \in \Omega$ is considered a specific combination of process parameters. The type of printing technology employed determines the level of dimensionality n; for instance, $\boldsymbol{x}$ might encompass extrusion temperature, print speed, layer height, and infill density for FDM, thus $n = 4$. Given the multi-faceted nature of quality control in pharmaceutical manufacturing, consider m distinct objectives $f_i: \Omega \to R$ for $i \in \{1,2,\dots,m\}$, each quantifying a critical quality attribute. The multi-objective optimization problem is presented in Eqs. 1 to 3.

$$min_{x\in\Omega} F(fx) = \left(f_1(x), f_2(x), \dots, f_m(x)\right)^{\top} \quad (1)$$

$$subject\ to\ g_j(x) \leq 0, j = 1,2,\dots,J \quad (2)$$

$$h_k(x) = 0, k = 1,2,\dots,K \quad (3)$$

where g_j and h_k represent inequality and equality constraints, respectively, encompassing regulatory requirements, physical limitations, and material properties. The solution to this problem is not a single point but rather a set of Pareto-optimal solutions, $P \subset \Omega$where no objective is improved without degrading at least one other objective.

For pharmaceutical 3D printing, the following specific objectives apply:

$$f_1(x) = \frac{1}{N}\sum_{i=1}^{N}\left|C_i(x) - C_{target}\right| \quad (API\ Content\ Accuracy) \quad (4)$$

$$f_2(x)0 = \sqrt{\frac{1}{N-1}\sum_{i=1}^{N}\left(C_i(x) - \bar{C}(x)\right)^2} \quad (Content\ Uniformity) \quad (5)$$

$$f_3(x) = -\sigma_{mech}(x)\ (Mechanical\ Strength) \quad (6)$$

$$f_4(x) = T_{total}(x)\ (Production\ Time) \quad (7)$$

$$f_5(x) = \int_0^{T\,diss}\left|D_{actual}(t;x) - D_{target}(t)\right|dt \quad (Dissolution\ Profile\ Accuracy) \quad (8)$$

where $C_i(x)$ represents the API content at the $i-th$ sampling point, $\bar{C}(x)$ is the mean content across all sampling points, $\sigma_{mech}(x)$ denotes the tensile strength of the printed formulation, $T_{total}(x)$ is the total production time, and $D_{actual}(t;x)$ and $D_{target}(t)$ are the actual and target dissolution profiles, respectively.

Mathematical model

To establish a quantitative relationship between process parameters and quality attributes, a multi-physics model integrating material behavior, heat transfer, and mass transport was developed. For FDM-based pharmaceutical printing, temperature distribution within the printed structure during fabrication is governed by the heat equation.

$$\rho\, c_p \frac{(\partial\, T)}{\partial\, t} = \nabla \cdot\ (k\, \nabla\, T)\ +\ Q \quad (9)$$

where ρ is the density, c_p is the specific heat capacity, k is the thermal conductivity, and Q represents heat sources/sinks. The flow behavior of the molten polymer-drug mixture through the nozzle is described by the Hagen-Poiseuille equation for non-Newtonian fluids:

$$Q_v = \frac{\pi\, R^4 \Delta\, P}{8\eta\, L} \cdot \left(\frac{3n+1}{4n}\right) \quad (10)$$

where Q_v is the volumetric flow rate, R is the nozzle radius, ΔP is the pressure differential, L is the nozzle length, η is the viscosity, and n is the flow behavior index. For API distribution within the printed structure, we employed a convection-diffusion model:

$$\frac{\partial\, C}{\partial\, t} + v \cdot \nabla\, C = D\, \nabla^2\, C + S \quad (11)$$

where C is the local drug concentration, v is the velocity field during printing, D is the diffusion coefficient, and S represents source/sink terms.
The mechanical properties of the printed formulation were modeled using a modified Gibson-Ashby relationship accounting for infill pattern and density:

$$\sigma_{mech}(x) = \sigma_0 \cdot \left(\frac{\rho(x)}{\rho_0}\right)^n \cdot \Psi(\theta, \phi) \quad (12)$$

where σ_0 represents the solid materials' strength, $\frac{\rho(x)}{\rho_0}$ represents the relative density as determined by the infill parameters, n represents an exponent determined by the material, and $\Psi(\theta, \phi)$ represents a function accounting for the anisotropic effects of print orientation angles θ and ϕ.

A modified Korsmeyer-Peppas equation used to model the drug release kinetics is presented in Eq 13.

$$\frac{M_t}{M_\infty} = k\, t^n + \xi(x) \quad (13)$$

where $\frac{M_t}{M_\infty}$ represents fractional drug release at time t, k is the release rate constant, n is the release exponent indicating the release mechanism, and $\xi(x)$ is a correction term that captures parameters' influence on the drug release profile.

NSGA-II Algorithm

The formulated MOO problem was solved using the NSGA-II, known for efficiency in sustaining diversity among Pareto-optimal solutions (Algorithm 1).

Details of the NSGA-II implementation steps

Chromosome representation

Each solution $x \in \Omega$ is encoded as a real-valued vector, with each element corresponding to a given parameter. A typical chromosome for FDM printing is given in Eq 14.

$$x = \left[T_{ext}, v_{print}, h_{layer}, \rho_{infill}, \omega_{drug} \ldots.\right]^{\mathsf{T}} \quad (14)$$

where T_{ext} is the extrusion temperature, v_{print} is the print speed, h_{layer} represents layer height, ρ_{infill} represents infill density, and ω_{drug} represents the percentage of drug loading.

Initialization

During the initialization step, the first step was to generate the initial population, P_0, using Latin Hypercube Sampling (LHS). This ensured uniform representation of the parameter space, Ω. Furthermore, each parameter was restricted within physically meaningful bounds (Eq 15).

$$x_{min} \leq x \leq x_{max} \quad (15)$$

Selection mechanism

This stage involved the binary tournament selection mechanism. Here, 2 individuals were randomly selected, with the parent being the one with better fitness (lower rank or, if ranks are equal, larger crowding distance). The pressure of the selection process drove the population toward the Pareto front while ensuring diversity.

Genetic operators

Crossover, a genetic operator, was performed using the Simulated Binary Crossover (SBX), and the distribution index was set at $\eta_c = 20$ (Eq 16).

$$c_{1,j} = 0.5\left[\left(1 + \beta_j\right)p_{1,j} + \left(1 - \beta_j\right)p_{2,j}\right] \quad (16)$$

where $p_{1,j}$ and $p_{2,j}$ are the j-th parameters of the parent solutions, $c_{1,j}$ and $c_{2,j}$ represent related offspring parameters; β_j represents a sample from a probability distribution derived from η_c.

Polynomial mutation was applied for mutation, and the distribution index was set at $\eta_m = 20$ (Eq 17).

$$c_j' = c_j + \delta_j \cdot (x_{j,max} - x_{j,min}) \quad (16)$$

where δ_j is a perturbation factor sampled from a polynomial distribution centered at zero with scale determined by η_m.

Design and analysis

Setup

A wide range of experiments were performed with the NSGA-II to validate the MOO framework, aimed at solving the QC problems in 3D printing pharmaceuticals. The experimental design was systematic and tested the capability of the proposed methodology with various process parameters and objectives.

Algorithm 1: NSGA-II for Pharmaceutical 3D-Printing Optimization

S/N	Operation
1	Initialize population P_0 of size N by sampling from Ω
2	Evaluate objective functions $F(x)$ for each $x \in P_0$
3	Apply non-dominated sorting to assign rank $r(x)$ to each $x \in P_0$
4	Calculate crowding distance d(x) for each $x \in P_0$
5	for $g = 1$ to G_{max} do
6	Select parents from P_{g-1} using binary tournament selection based on rank and crowding distance
7	Generate offspring population Q_g through SBX crossover and polynomial mutation
8	With probabilities p_c and p_m
9	Evaluate objective functions F(x) for each $x \in Q_g$
10	Form combined population $R_g = P_g - 1 \cup Q_g$
11	Apply non-dominated sorting to assign ranks to individuals in R_g
12	Initialize new population $P_g = \emptyset$
13	$i = 1$
14	while $\|Pg\| + \|Fi\| \leq N$ do
15	Calculate crowding distance for each individual in F_i
16	$P_g = P_g \cup F_i$
17	$i = i + 1$
18	end while
19	Sort Fi in descending order of crowding distance
20	Add the first (N −|Pg|) elements of Fi to Pg
21	end for
22	$P = \{x \in P_{G_{max}} \mid r(x) = 1\}$
23	return P

Input: Population size N, maximum generations $G_{\max}$, crossover probability p_c, mutation probability p_m Output: Pareto-optimal set P

Parameter selection

Six key process parameters that significantly influence the quality attributes of 3D-printed pharmaceuticals were considered in the proposed MOO framework. They were:

Extrusion temperature ((T_{ext})): $160 - 220°C$

Print speed (v_{print}): 10 – 60 mm/s

Layer height (h_{layer}): 0.1–0.3 mm

Infill density (ρ_{infill}): 0.2 – 0.8
Drug loading (ω_{drug}): 0.05 – 0.3

Print orientation: $0 - 90°$

Selection of these parameters was backed by a literature review, as they have been previously established as factors that impact critical quality attributes; the ranges of the parameters were set based on preliminary experiments and existing literature on FDM-based pharmaceutical printing [10–12].

Objective functions

Five interacting targets were examined, including the drug concentration precision (unfitting from the optimum dose of 100 mg), homogeneity of content (drug concentration standard deviation), mechanical properties (printed dosage form tensile strength), printing time (time needed to print the dosage form) and release profile precision (unfitting from the optimum dissolution curve). These objectives were considered simultaneously to align with the proposed mathematical formulation in this study.

Algorithm configuration

The NSGA-II algorithm was configured with the following parameters: population size = 100, maximum generations = 100, crossover probability = 0.9, mutation probability = 1/6, distribution index for crossover (η_c) = 20, and distribution index for mutation (η_m) = 20. The initial population was generated using LHS to ensure comprehensive exploration of the parameter space and uniform coverage across all dimensions.

The algorithm's convergence was monitored using the hypervolume indicator, which quantifies both diversity and proximity of solutions to the true Pareto front.

RESULTS

Content distribution

Solution 1 (blue) showed the smallest variation (i.e., accuracy) from the target value of 100 mg, suggesting that this solution has better content accuracy and uniformity under moderate extrusion temperature (around 185 ℃), low print speed (25 mm/s), and medium layer height (0.18 mm). Solutions 2 and 3 (orange and yellow) showed a larger content range, with higher mean responses (103 mg and 105 mg, respectively; Figure 3).

Mechanical properties

Solution 1 consistently exhibited superior mechanical properties at all infill densities, with 15 % higher mechanical properties than solutions 2 and 3 at the same average infill density. These suggest that solution 1 reached a maximum stress of around 32 MPa, while solutions 2 and 3 reached 27 MPa and 28 MPa, respectively (Figure 4).

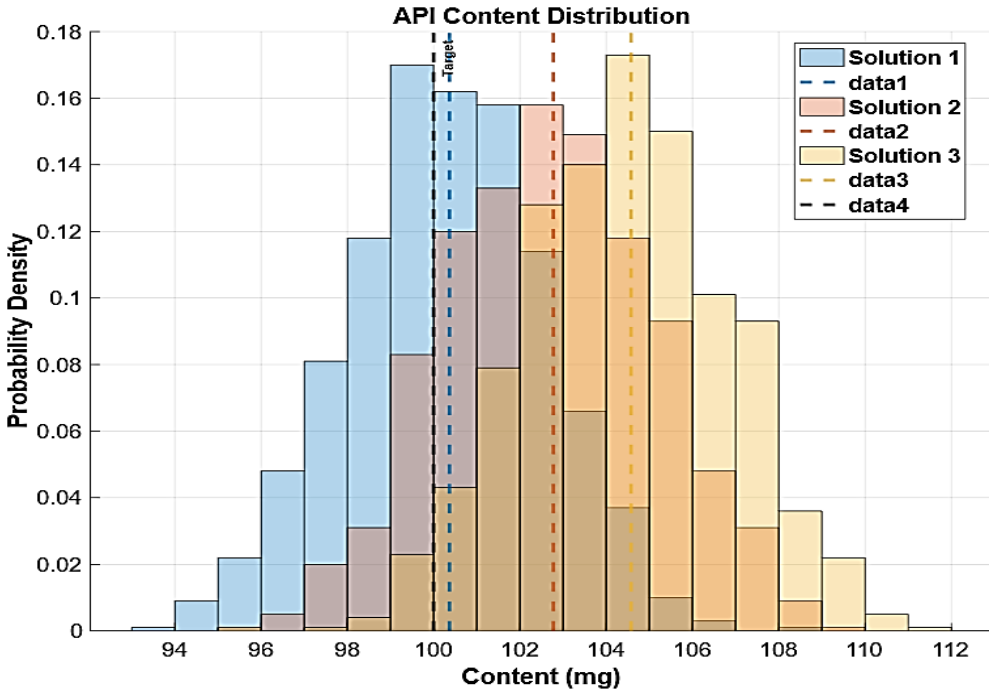


Figure 1: Content distribution of API for three Pareto-optimal solutions compared to target content (100 mg)

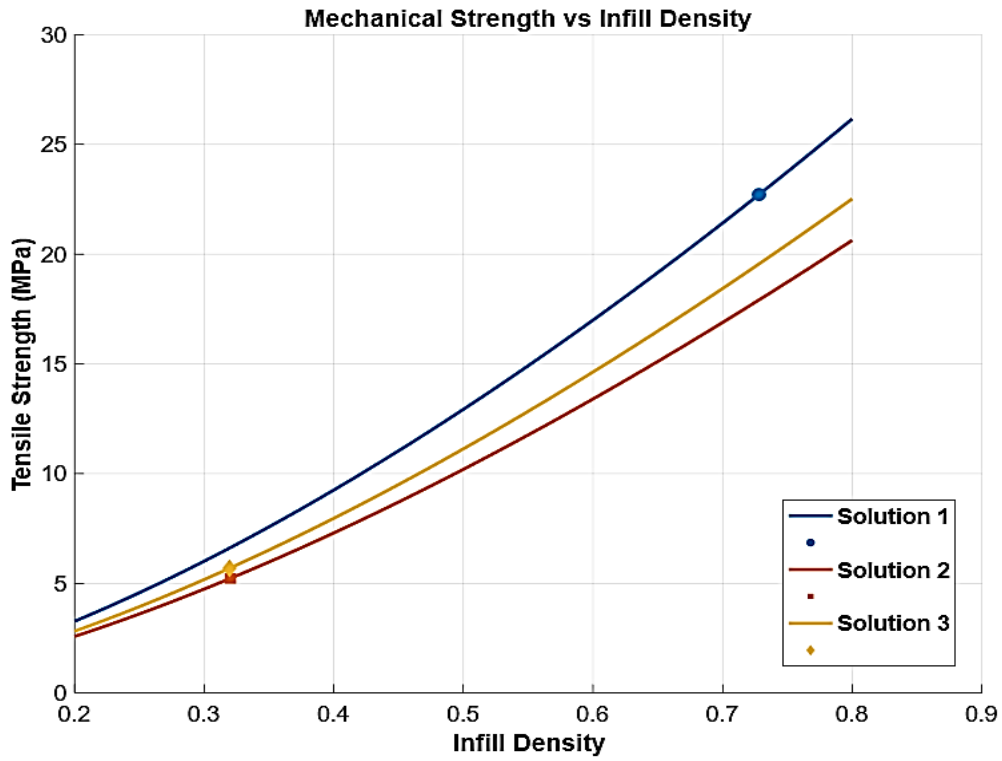


Figure 2: Relationships between infill density and mechanical strength for three Pareto-optimal solutions

Dissolution profile

None of these three solutions has a dissolution profile very close to the target first-order release profile. The target profile (dashed black line) has a first-order release pattern with a gradual slope to 90 % release at 24 h. Solution 1 (blue) has a very low rate of release, giving approximately 20 % after 24 h. Solutions 2 and 3 (orange and yellow) were graphically similar, with substantially faster release rates (over 80 % at 24 h) than Solution 1, but less than the target 90 % (Figure 5).

Production efficiency

The result revealed the expected inverse relationship between layer height and production time. In both solutions, production time decreases as layer height increases, and they show a step-like behavior due to discrete changes in the number of layers that will be produced as the height of a layer increases. For example, solution 1 (blue) always has longer build times than solution 3 (yellow), especially at small layer heights. Solution 1 needs around 175 – 200 s to produce at 0.1 mm layer height and 150 – 175 s for Solution 3 (Figure 6).

Parameter configuration and quality trade-offs

Solution 1 (blue) showed a medium-thickness layer (0.18 mm height), medium infill density, low print speed, and low orientation angle, while solutions 2 (orange) and 3 (yellow) reflected the use of higher printing speeds, higher extrusion temperatures, higher drug loads, and different rotation angles adopted. The only compromises in 3D printing drugs for human consumption were explained by the quality trade-off radar chart (Figure 7). Solution 1 (blue) represents an excellent solution for mechanical performance. It exhibited good content uniformity but had significantly less dissolution profile accuracy and a longer production time. Solution 3 (yellow) showed the lowest content accuracy and shortest production time. Solutions 2 and 3 have a similar trend in most of the objectives (Figure 8).

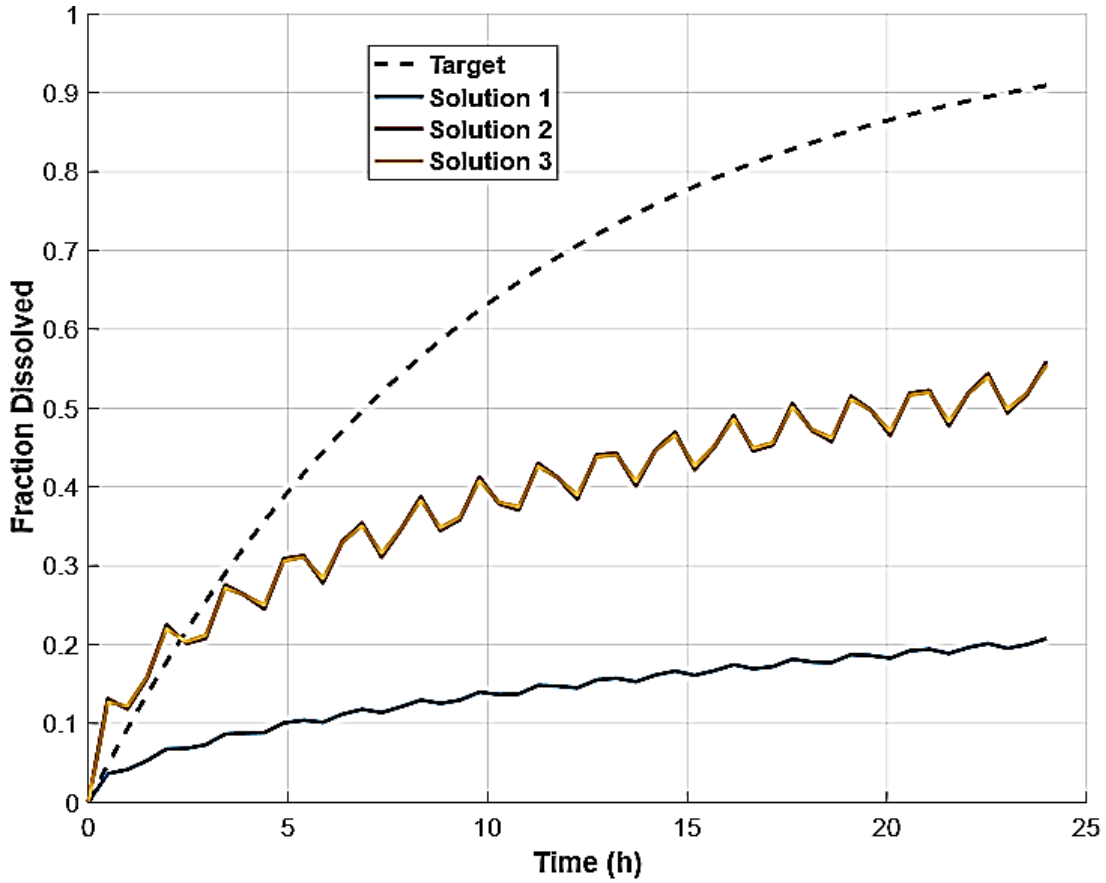


Figure 3: Dissolution profiles for three Pareto-optimal solutions compared to the target first-order release profile (dashed line)

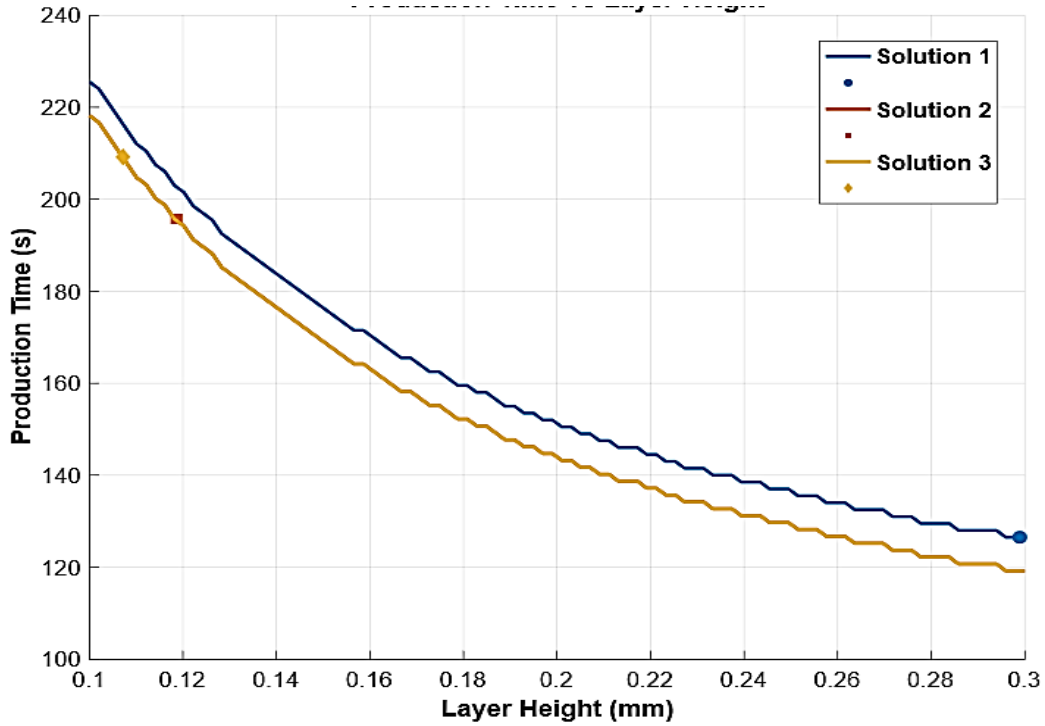


Figure 4: The layer height-production time relationship for three Pareto-optimal solutions

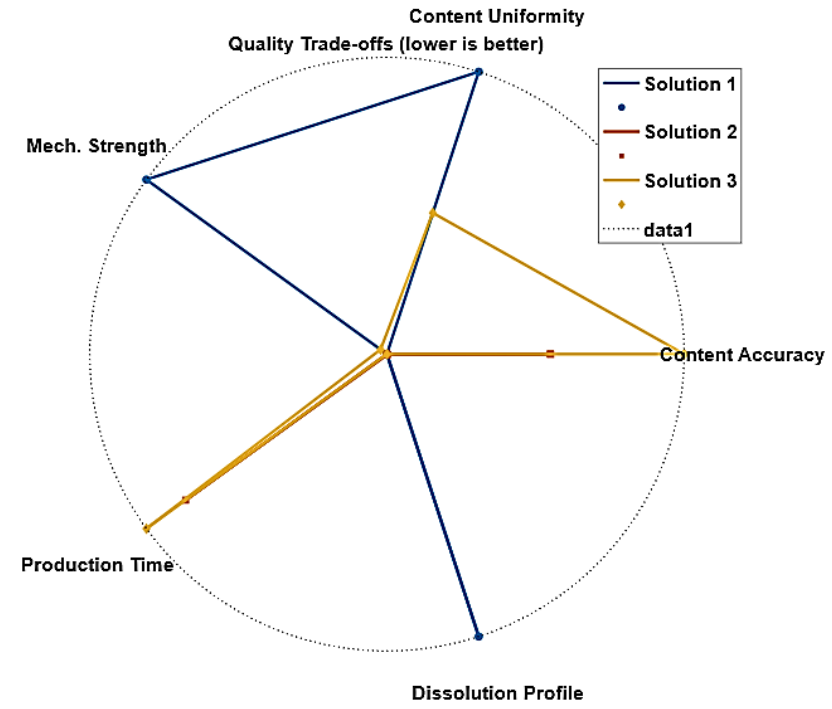


Figure 7: Radar chart depicting trade-offs between quality attributes for three Pareto-optimal solutions

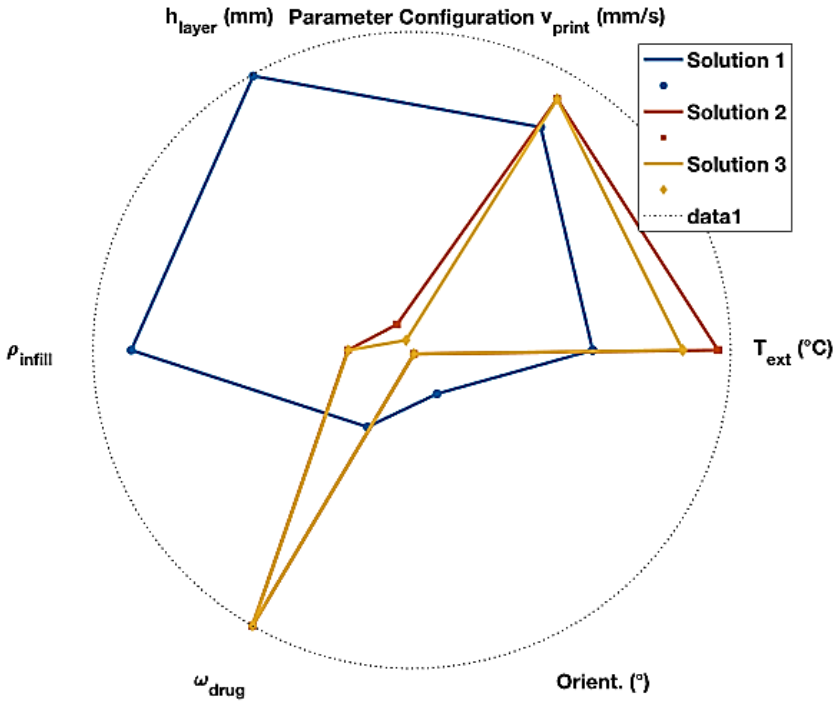


Figure 8: Radar chart showing parameter configurations for three Pareto-optimal solutions

Hypervolume convergence and algorithm performance

NSGA-II achieved approximately 85 % of the theoretical maximum hypervolume by generation 80, with improvements declining from about 2.5 % per generation in the first 30 generations to < 0.5 % after generation 60. Validation predictions were within 12 % of experimental values, except for dissolution profile accuracy, which varied by approximately 25 %.

DISCUSSION

There were obvious differences in API content distribution across different parameter combinations, indicating more variability and systematic overestimation of the dose [13]. The solutions focused on production speed and faster production time, as well as on temperature and higher print speed. The noticed differences may be caused by the conflict between processing variables, specifically the influence of the speed of printing and the setting temperature of the extruder head on the melt rheology of the polymer. Increasing the extrusion temperature reduces the viscosity of the molten mixture, which may cause drug degradation. Additionally, as the speed of printing increases, problems of melt deposition inconsistency will arise. Therefore, these interactions affect the nature of the relationship between 3D printing efficiency and the accuracy of the dose [14,15]. The superiority of Solution 1 in mechanical properties may be attributed to a near-optimum extrusion temperature for mechanical integrity of the printed structure (185 ˚C) or the existence of the most favorable print orientation with less anisotropic weakness in the printed structure. The results are in agreement with the primary influence of infill density on mechanical strength, influenced by processing parameters like the temperature of the extrusion and the orientation [16].

The reduced thickness of the layers will lead to increased interface between printed layers, which promotes water penetration and subsequent drug dissolution. Again, reduced infill densities will leave more void spaces in the structure, which enlarges the dissolution surface area. The oscillation in solutions 2 and 3 indicated that the correction term in the modified Korsmeyer-Peppas model is a good representation of the effect of process parameters on release kinetics. The results collectively suggest that although process parameter optimization is a key strategy to control dissolution profiles, there are other options (such as the addition of modifiers to the powder blend or post-processing procedures) that should be explored to attain the desired dissolution characteristics [17]. This difference in production times may be attributed to variation in printing speeds of the solutions. This is relevant for point-of-care manufacturing scenarios, when time may be critical for production. The results showed that when production is accelerated by printing speed or the height of the layers, content uniformity and dissolution control were reduced compared to lower production speed. This essentially highlights the need for multi-objective optimization to find suitable compromises related to clinical needs in pharmaceutical 3D printing [18].

Visualization of parameter configuration and quality trade-offs focuses on data showing that a particular solution may not satisfy all quality attributes ideally, and selection should be based on context and product attributes. The convergence pattern from the dissolution kinetic model indicates effective exploration and exploitation of the parameter space and a well-distributed Pareto-optimal solution set, while the validation results support the reliability of the mathematical models.

CONCLUSION

This study has designed a potential multi-objective optimization approach for quality attributes involved during the development of dosage forms and drug delivery systems using 3D-printing technologies. It focused on the critical role of enhancing several quality parameters rather than monitoring single variables. The approach is therefore providing a general framework for enhancing the final characteristics of the personalized dosage forms while maintaining its flexibility. Future studies should extrapolate this model to other printing technologies such as stereolithography (SLA) and selective laser sintering (SLS), incorporate real-time quality monitoring and adaptive control, and integrate regulatory requirements directly into optimization objectives to support commercial-scale manufacturing.

DECLARATIONS

Acknowledgement/Funding

The authors gratefully acknowledge the support provided by the College of Pharmacy of the University of Basrah, Al-Kunooze University, and the Ministry of Oil, Iraq.

Use of Artificial intelligence/Large language models

The authors confirm that AI-based tools were used solely for language editing and manuscript polishing purposes (e.g., grammar, phrasing, and clarity). All intellectual contributions, study analyses, and interpretations reported in the manuscript are the original work of the authors.

Availability of data and materials

The datasets used and/or analyzed during the current study are available from the corresponding author on reasonable request.

Conflict of interest

No conflict of interest is associated with this work.

Contribution of authors

We declare that this work was done by the author(s) named in this article, and all liabilities pertaining to claims relating to the content of this article will be borne by the authors.

REFERENCES

1. *Bernatoniene J, Stabrauskiene J, Kazlauskaite JA, Bernatonyte U, Kopustinskiene DM. The future of medicine: how 3D printing is transforming pharmaceuticals. Pharmaceutics 2025; 17(3): 390. doi: 10.3390/pharmaceutics17030390.*
2. *Sun S, Alkahtani ME, Gaisford S, Basit AW, Elbadawi M, Orlu M. Virtually possible: enhancing quality control of 3D-printed medicines with machine vision trained on photorealistic images. Pharmaceutics 2023; 15(11): 2630. doi: 10.3390/pharmaceutics15112630.*
3. *Cui M, Pan H, Su Y, Fang D, Qiao S, Ding P, et al. Opportunities and challenges of three-dimensional printing technology in pharmaceutical formulation development. Acta Pharm Sin B 2021; 11(8): 2488-2504. doi: 10.1016/j.apsb.2021.03.015.*
4. *Yang TL, Szewc J, Zhong L, Leonova A, Giebułtowicz J, Habashy R, et al. The use of near-infrared as process analytical technology (PAT) during 3D printing tablets at the point-of-care. Int J Pharm 2023; 642: 123073. doi: 10.1016/j.ijpharm.2023.123073.*
5. *Sierra-Vega NO, Ashraf M, O'Connor T, Kopcha M, Di Prima M, Coburn J, et al. Emerging 3D printing technologies for solid oral dosage forms: processes, materials and analytical tools for real-time assessment. Int J Pharm 2025; 673: 125415. doi: 10.1016/j.ijpharm.2025.125415.*
6. *Deb K, Pratap A, Agarwal S, Meyarivan T. A fast and elitist multiobjective genetic algorithm: NSGA-II. IEEE Trans Evol Comput 2002; 6(2): 182-197. doi: 10.1109/4235.996017.*
7. *Zhang Q, Li H. MOEA/D: a multiobjective evolutionary algorithm based on decomposition. IEEE Trans Evol Comput 2007; 11(6): 712-731. doi: 10.1109/TEVC.2007.892759.*
8. *Elbadawi M, McCoubrey LE, Gavins FKH, Ong JJ, Goyanes A, Gaisford S, et al. Harnessing artificial intelligence for the next generation of 3D printed medicines. Adv Drug Deliv Rev 2021; 175: 113805. doi: 10.1016/j.addr.2021.05.015.*
9. *Budzik G, Woźniak J, Paszkiewicz A, Przeszłowski Ł, Dziubek T, Dębski M. Methodology for the quality control process of additive manufacturing products made of polymer materials. Materials (Basel) 2021; 14(9): 2202. doi: 10.3390/ma14092202.*
10. *Alhijjaj M, Nasereddin J, Belton P, Qi S. Impact of processing parameters on the quality of pharmaceutical solid dosage forms produced by fused deposition modeling (FDM). Pharmaceutics 2019; 11(12): 633. doi: 10.3390/pharmaceutics11120633.*
11. *Dumpa N, Butreddy A, Wang H, Komanduri N, Bandari S, Repka MA. 3D printing in personalized drug delivery: an overview of hot-melt extrusion-based fused deposition modeling. Int J Pharm 2021; 600: 120501. doi: 10.1016/j.ijpharm.2021.120501.*
12. *Elkasabgy NA, Mahmoud AA, Maged A. 3D printing: an appealing route for customized drug delivery systems. Int J Pharm 2020; 588: 119732. doi: 10.1016/j.ijpharm.2020.119732.*
13. *Skowyra J, Pietrzak K, Alhnan MA. Fabrication of extended-release patient-tailored prednisolone tablets via fused deposition modelling (FDM) 3D printing. Eur J Pharm Sci 2015; 68: 11-17. doi: 10.1016/j.ejps.2014.11.009.*
14. *Shimelis TG, Abraham DW. Characterization and effects of process parameters on the mechanical, microstructural, and thermal behavior of PEEK in fused deposition modeling 3D printing. Results Mater 2025; 28: 100833. doi: 10.1016/j.rinma.2025.100833.*
15. *Nasereddin JM, Wellner N, Alhijjaj M, et al. Development of a simple mechanical screening method for predicting the feedability of a pharmaceutical FDM 3D printing filament. Pharm Res 2018; 35: 151. doi: 10.1007/s11095-018-2432-3.*
16. *Syrlybayev D, Zharylkassyn B, Seisekulova A, Akhmetov M, Perveen A, Talamona D. Optimisation of strength properties of FDM printed parts—a critical review. Polymers (Basel) 2021; 13(10): 1587. doi: 10.3390/polym13101587.*
17. *Vojinović A, Medarević Đ, Stanojević G, Mirković D, Mugoša S, Adamov I, et al. Development and evaluation of 3D-printed losartan potassium tablets using semi-solid extrusion: the effect of geometry, drug loading and superdisintegrant. Pharmaceuticals (Basel) 2025; 18(10): 1504. doi: 10.3390/ph18101504.*
18. *Pires FQ, Alves-Silva I, Pinho LAG, Chaker JA, Sa-Barreto LL, Gelfuso GM, et al. Predictive models of FDM 3D printing using experimental design based on pharmaceutical requirements for tablet production. Int J Pharm 2020; 588: 119728. doi: 10.1016/j.ijpharm.2020.119728.*